Advanced Bathymetric Survey Using The Yellowscan Navigator: Applications in Erosion and Soil Movement Tracking.

Johann Berthelot[1], Alexandre Gintz[1], Pol Kennel[1] , Nassim Doukkali[1] and Tristan Allouis[1]

[1] Yellowscan, 525 Avenue Saint Sauveur du Pin, 34980 Saint-Clément-De-Rivière, France - (johann.berthelot@yellowscan.com)

Keywords: Green Laser Bathymetry, UAV, Hydrodynamic, Environmental Monitoring

Abstract

In this paper, we present a practical application of a new bathymetric LiDAR sensor mounted on an unmanned aerial vehicle (UAV). Using the YellowScan Navigator, we conducted four data acquisition campaigns over the Herault River, each during different seasons. All flights followed the same plan, using the same UAV and sensor configuration to ensure consistency. This multi-temporal dataset allows us to monitor riverbed changes with a vertical accuracy of several centimeters. Our results demonstrate the sensor's capability to detect subtle morphological variations in the riverbed, bridging the gap between traditional multi-echo sonar techniques and topographic LiDAR systems. This new tool offers a valuable addition to the geodetic toolbox for fluvial and environmental monitoring.

1. Introduction

Green LiDAR bathymetry, an active remote sensing technique, has seen significant advances in recent years, particularly with the miniaturization of sensors and their integration into UAV platforms (Zuckerman (2019); Mandlburger et al. (2020); SBG Systems (2025); Quadros and Keysers (2018); Wilder Young (2017); Kinzel and Legleiter (2019); Mitchell (2019); Gangelhoff et al. (2023)). This technology enables the acquisition of high resolution topographic and bathymetric data in shallow water environments, offering a valuable alternative to traditional methods such as sonar or photogrammetry, which are often limited by accessibility, water clarity, or spatial resolution Szafarczyk and Toś (2023).

Green LiDAR systems, such as the YellowScan Navigator, operate using a 532 nm wavelength laser, which penetrates the water column to measure depths with high precision. Unlike infrared-based topographic LiDAR, green LiDAR can capture both the water surface and submerged terrain, making it ideal for mapping riverbeds, estuaries, and coastal zones (Szafarczyk and Toś (2023); Mandlburger et al. (2016b); Fernandez-Diaz et al. (2014); Mandlburger et al. (2016a); Lague and Feldmann (2020)). The ability to collect dense point clouds with excellent vertical accuracy allows for detailed morphological analysis of fluvial systems, including sediment transport, erosion, and deposition processes (Fernandez-Diaz et al. (2014)).

In addition to its technical capabilities, UAV-based green LiDAR offers logistical advantages. It enables rapid deployment, flexible flight planning, and access to remote or ecologically sensitive areas where ground-based surveys are impractical or invasive. This makes it particularly suitable for repeated monitoring campaigns, which are essential for understanding seasonal dynamics and long-term trends in river systems.

In this study, we evaluated the performance of the YellowScan Navigator for bathymetric mapping and terrain change detection on the Herault River, focusing on the site known as *Plage du Pont du Diable*. During four acquisition campaigns conducted across different seasons, we maintained consistent flight parameters to ensure comparability. The resulting datasets reveal terrain modifications linked to hydrological activity, with detectable changes ranging from several centimeters to over a meter. These findings underscore the potential of UAV-based green LiDAR as a bridge technology between traditional multiecho sonar and topographic LiDAR, filling a critical gap in geodetic and environmental monitoring workflows.

2. Instrumentation and Data Handling

2.1 Green Lidar system: Yellowscan Navigator

The YellowScan Navigator is a cutting-edge bathymetry LiDAR system specifically developed for use with UAVs, making it ideal for mapping coastal and river environments. This new Lidar offers the capability to fly at 80m AGL (above ground level), as the other solutions are limited to 20 meters. This advanced system includes a laser scanner that has been developed in-house by YellowScan to ensure high performance and accuracy. The Navigator can reach depth up to 18 meters in exceptionally clear water conditions. The main specifications of the system and a view of it are presented in table1 and Figure 1.

Specification	Value
Wavelength	532nm
Pulse repetition rate	20 kHz
Pulse width	0.8 ns
Recommanded AGL	80m
Footprint	30 cm @ 80m AGL
Max Depth	2 secchi
Weigth	4.2 kg battery included
Precision	3 cm
Accuracy	3 cm
Field of view	40°
Scan pattern	Ellipse
Dimensions	L 35 x W 16 x H 19 cm

Table 1. Table of the main specification of the Yellowscan Navigator

2.2 UAV platform

The Navigator system is mounted on a DJI M600 pro drone, with a special gremsy mount support. This UAV (Unnamed

Figure 1. Picture showing the Yellowscan Navigator

Airborne Vehicle) can carry up to 4.5 kg for a flight endurance of 15 min. Throughout the study, the position of the Lidar mounting system has been kept fixed. In this way the mounting lever-arms for trajectory processing are always the same and remained fixed relative to the GNSS antenna. The flight plan has been performed using UGCS software.

2.3 Data processing

The processing has been performed with the Yellowscan Cloudstation software. The Yellowscan Navigator is recording full-wave signals, requiring a specific data processing in order to get the final points cloud. For each dataset, the processing time in high-resolution mode took 2 hours on a descent computer. We used a Gaussian mixture decomposition to extract the information encoded in the full wave (Kim et al. (2023)). This approach, along with others, facilitates improved extraction of the waterbed echoes. The datas have been processed following the specific pipeline presented in Fig.2.
A typical example of the signal acquired by the system is diplayed in Figure 2b, after the preprocessing step. We used a value of n_{water}=1.33 for the refraction as we were in fresh-water. We used a simple model for the refraction correction described in (Feldmann (2018)).

3. Results

The study area, called *Plage du pont du diable*, is located in the south of France, near Montpellier. The Herault River forms here a picturesque lake-like area that is popular for swimming, sunbathing, and boating. The site is notable for its ecological importance, with diverse flora and fauna inhabiting the surrounding area. The steep banks and clear waters of the Herault River provide an ideal environment to study erosion and soil movement, making it a valuable location for environmental research. We conducted 4 surveys at different dates on this location (cf. Figure 3). All acquisitions have been made with the same system and the same flight plan. We decided to fly 80 meters above the ground with a speed of 5 m/s and an overlap between the strips of 60%. All flights were conducted in the same way to compare them. To have cm-precision of the direct

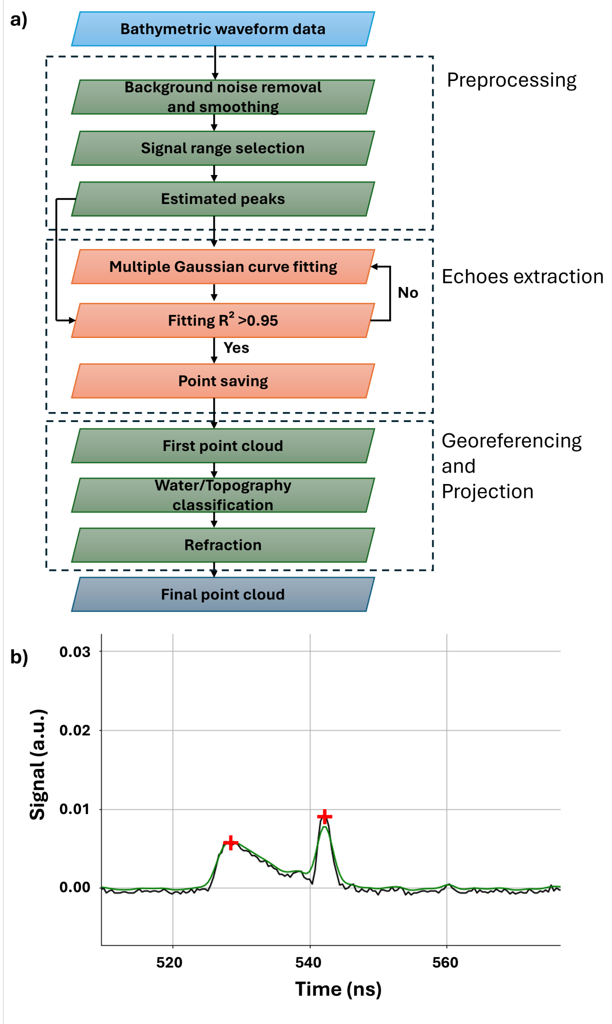

Figure 2. a) Workflow of the bathymetric data. b) Graphical example of a typical signal obtained after the preprocessing step. In black is represented the raw signal, in green the filtered signal and the red markers indicates the local maximums.

geo-referenced Lidar measurements, before each take-off and landing a special initialization procedure of the installed IMU was performed. The full flight takes 12 min including the initialization procedure.
We can already see that the water level between the 4 acquisitions is completely different as well as the water turbidity/clarity. In fact, three flights over the fourth had good weather and water conditions. However, the acquisition of march 2025 was made during a meteorological event. This difference has been observed in the data set with the maximum depth detected under water. In the case of the 3 other surveys we could easily reach 4 meters penetration depth before losing the detection. For the last one, we could only reach 1.2 meters.
The flow of water is monitored by a station located upstream of the study site. With this information, we know the amount of water and, more specifically, when meteorological events occurred. The results are presented in Figure 4.

During the year difference between the first acquisition and the second one, the site has experienced more than 10 events (cf. Figure4). To compare all data and assess the evolution of the terrain, we used the M3C2 plugin (Lague et al. (2013)). Our data sets have been classified according to the Las 1.4 norm.

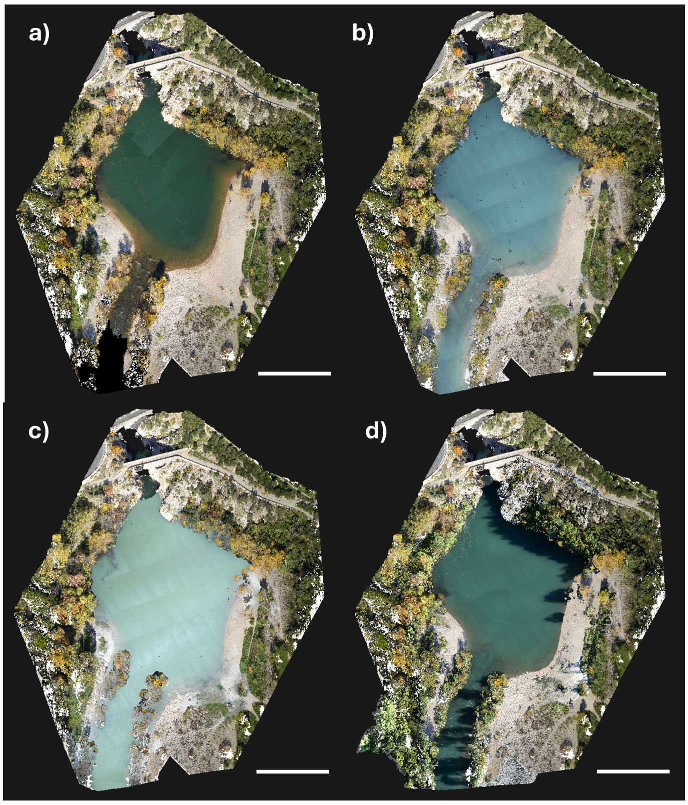

Figure 3. Colorized point clouds of the same geographical area captured at three different dates: a) November 2023, b) November 2024, c) March 2025, d) April 2025.

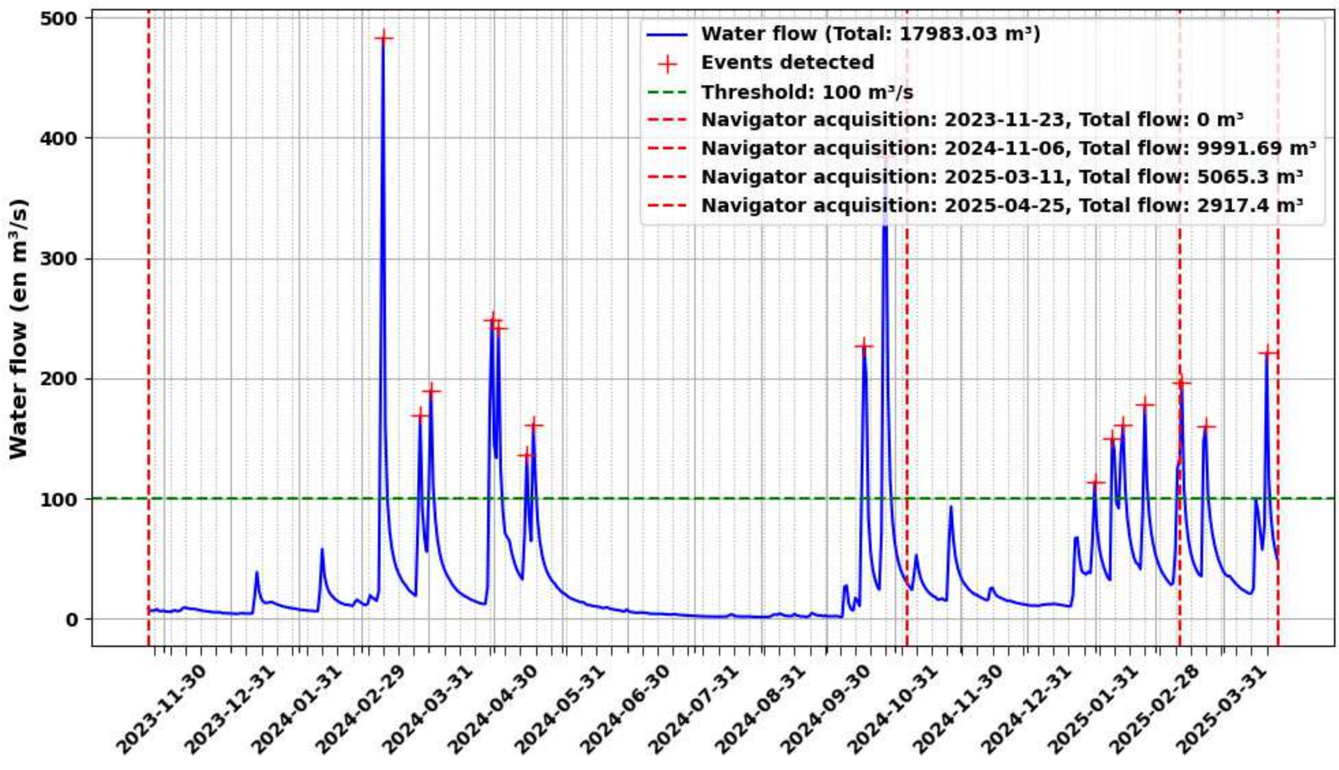

Figure 4. Graph depicting the water flow (m^3/s) from November 1, 2023, to April 25, 2025. The blue line represents the water flow per day, with several peaks marked by red points. Vertical dashed red lines indicate the date of bathymetry Lidar survey: November 2023, November 2024, March 2025 and April 2025. The scale represents 20m.

We kept only the points classified as 2 (topographic ground) and 40 (water ground) for this analysis.

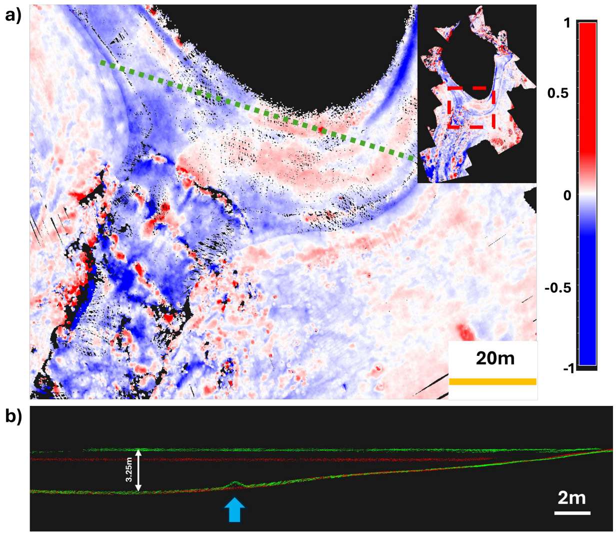

Figure 5. a) Graphical map of distance difference by the M3C2 method between November 2023 and November 2024 data set with only ground classified points (2 and 40). b) Cross section of 1 m wide over the bathymetry data from November 2023 (red) and November 2024 (green). The blue arrow shows the terrain change visible in a).

The result is presented in Figure 5a. The highest changes are mainly located near the main riverbed. Other changes are also present outside, but with lower amplitude. The most affected location is the canal reduction between the beach part and the river. We made a cross section at a location where a large localized modification is present (green line in Figure 5a). The result of the cross section is presented in Figure 5b. In red is plotted the point of the data from November 2023 and in green the data from November 2024. We have a good agreement for the floor data, except for one part indicated by the blue arrow.

In the case of data for March 2025 compared with the data obtained in November 2024 as a reference, we do not see much change. It is difficult to obtain modification onto the riverbed with this dataset, because of the higher water turbidity, we could not detect it (cf Figure8). However, we were able to nicely detect the water level. The difference in water surface height is 1.2 meters between November 2024 and March 2025, while the difference between November 2023 and November 2024 is only 70 centimeters. We have a good agreement between the ground points measured over the different datasets and will show discussed about if later. The March dataset, although valuable due to the high water level and increased turbidity, did not allow for a clear observation of the riverbed morphology. These limitations were addressed by the April 2025 dataset, which benefited from improved water clarity and more favorable acquisition conditions. By comparing the April 2025 data with that of November 2024, we were able to assess morphological changes in the riverbed over a five-month period. The results of this comparison, obtained using the M3C2 algorithm, are presented in Figure 7.

In this case, the observed changes in the riverbed were less pronounced than those detected in the previous annual comparison.

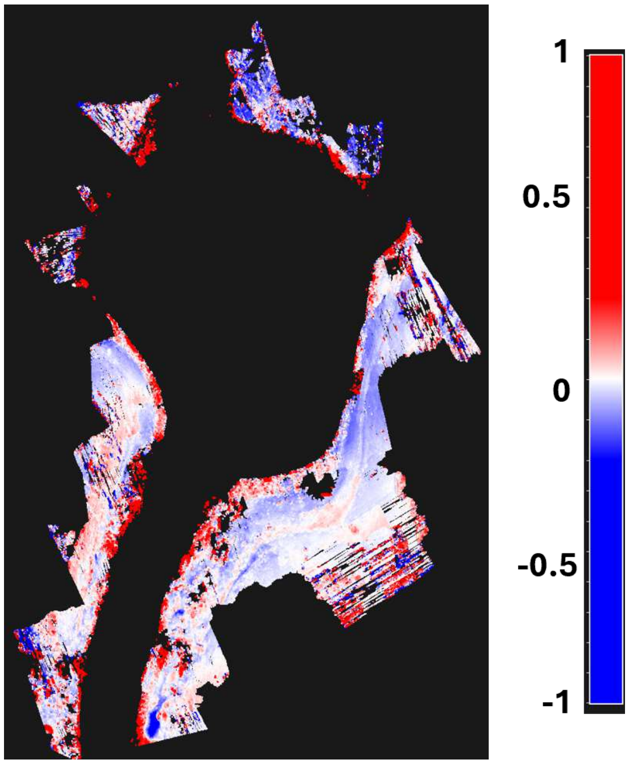

Figure 6. M3C2 graphical result from the bathymetry data of November 2024 as reference and March 2025.

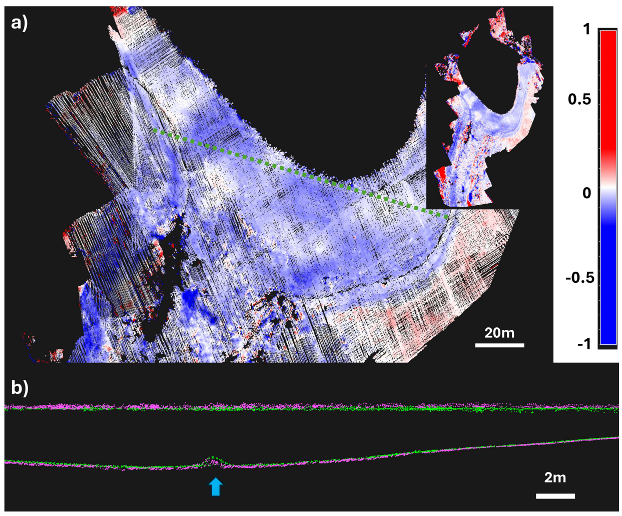

Figure 7. a) Graphical map of distance difference by the M3C2 method between November 2024 and April 2025 data set with only ground classified points (2 and 40). b) Cross section of 1 m wide over the bathymetry data from November 2024 (green) and April 2025 (purple). The blue arrow shows the presence of the rocks detected in Figure 5.

This difference can be attributed not only to the shorter time interval (five months versus one year), but also to the hydrological context. While, the total water volume between the two periods differed by only 20%, no major hydrological events occurred during the second interval (cf. Figure 4). This suggests that the intensity and frequency of high-energy events, rather than cumulative water volume alone, play a dominant role in driving significant morphological changes. Consequently, it is consist-

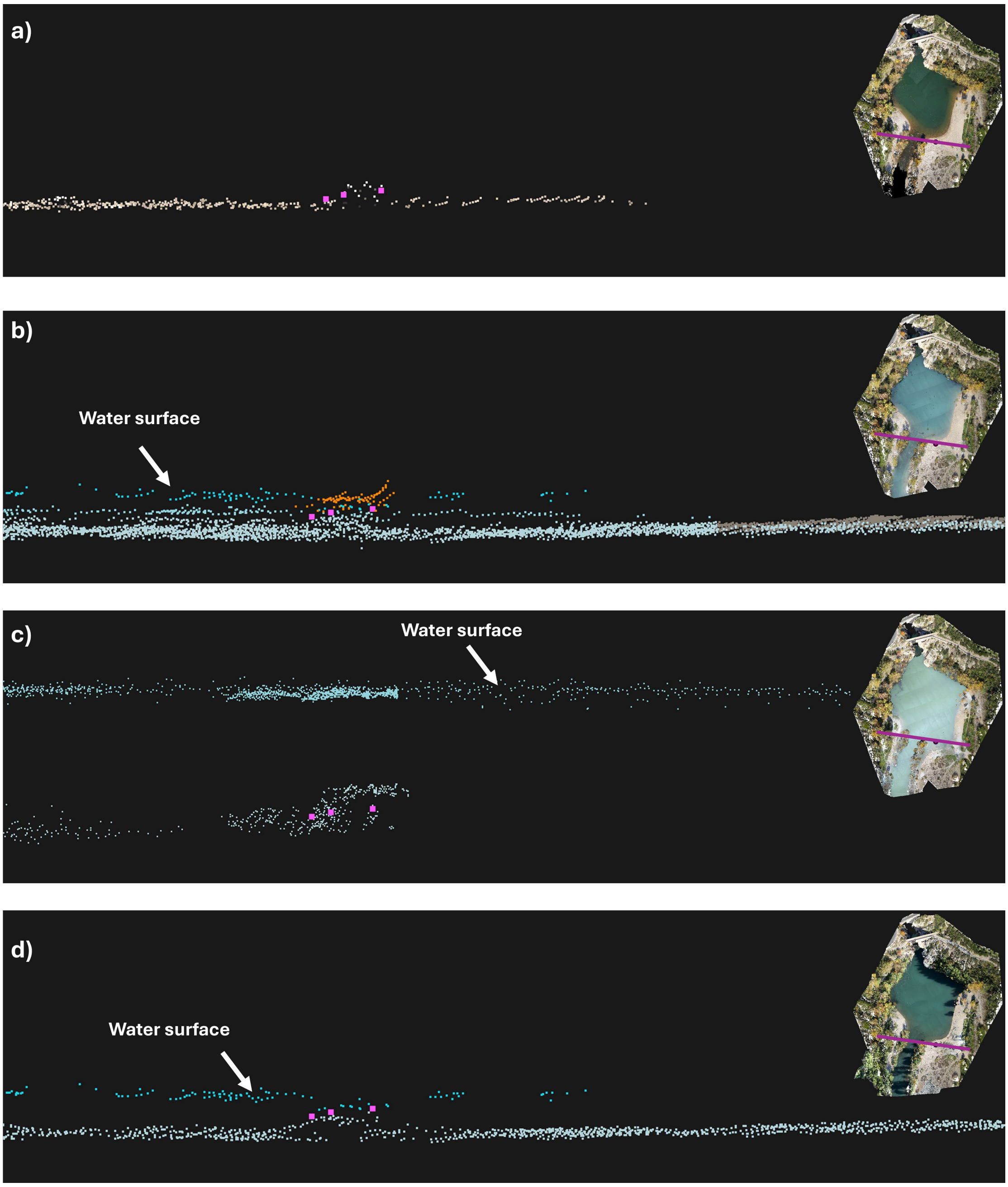

Figure 8. Cross section in the different point cloud for each acquisition at the same location. a) November 2023,b) November 2024, c) March 2025, d) April 2025. In each image the overview of the point cloud as well as the location of the cross section is represented. The water surface is indicated by the white arrow. Ground Control Points (GCPs) are in purple color.

ent to observe more substantial terrain modifications following more intense or extreme hydrological episodes.

By examining the rocks visible in the November 2024 point cloud, we observed that they were still present in the April 2025 dataset (see Figure 7b). However, a closer analysis reveals a slight displacement: the area containing the rocks has shifted approximately 15 cm vertically and about 5 cm horizontally. This displacement is likely due to the nature of the surrounding substrate, which is predominantly composed of sand material highly susceptible to movement under varying flow conditions. These subtle changes highlight the dynamic behavior of sedimentary environments and the importance of high-resolution temporal monitoring to capture such micro-morphological variations.

Finally we used some Ground control points (GCPs) in order to control the alignment and good matching of our dataset. This points are only used to verify the positioning and not to process the point clouds.

We made one cross section on a part where all the dataset and the GCPs were visible and were located also under the water. This points were taken on the top of rocks clearly visible. The result is visible in Figure 8.

For each acquisition, we consistently observe the same object, both submerged and exposed, depending on the water level at the time of the survey. Three ground control points (GCPs) are precisely positioned on the rock surface, providing reliable reference markers across all datasets. By analyzing the absolute distance between the GCPs and the corresponding LiDAR points, we found that the positional discrepancies remained below 3 cm for all acquisitions, demonstrating the high spatial accuracy of the system.

Interestingly, even in the March 2025 dataset, characterized by high water levels and turbidity, the object was still successfully detected. However, the most challenging conditions were encountered when the water level was just above the object. In such cases, the discrimination between the water surface, water column, and bottom echoes becomes particularly complex.

Moreover, the shape of the rock appears less defined when submerged, with noticeable variations in contour sharpness and surface texture. These differences are not due to actual morphological changes but rather to the interaction between the laser beam and the water medium. Such observations highlight the importance of considering environmental conditions when interpreting bathymetric LiDAR data, especially in shallow or transitional zones where water and terrain interact closely.

4. Conclusion

This study demonstrates the strong potential of the YellowScan Navigator, a cutting-edge UAV-mounted bathymetric LiDAR system, for high-resolution monitoring of riverbed dynamics. Our multi-temporal surveys over the Hérault River successfully captured terrain changes ranging from several centimeters to over a meter, confirming the system's precision and reliability in shallow water environments.

Looking ahead, future research could explore the integration of bathymetric LiDAR data with hydrodynamic models to better understand sediment transport and erosion processes. Additionally, combining LiDAR with multispectral or hyperspectral imagery could enhance the classification of submerged vegetation and substrate types. Expanding the use of this technology to diverse hydromorphological contexts—such as braided rivers, estuaries, or post-flood assessments—would further validate its versatility. Finally, the development of automated processing pipelines and machine learning approaches for change detection could significantly improve the efficiency and scalability of UAV-based bathymetric monitoring.

5. Acknowledgements

This work has been done in the framework of the project Alligator (FEDER OCC000787). The author would like to thanks the region Occitanie for they financial support through the program "Occitanie FEDER-FSE+ 2021-2027".

References

Feldmann, B., 2018. Étude des facteurs contrôlant la profondeur maximale de mesure bathymétrique par lidar aéroporté. Technical report, Université Toulouse Jean Jaurès. Internal report.

Fernandez-Diaz, J. C., Glennie, C. L., Carter, W. E., Shrestha, R. L., Sartori, M. P., Singhania, A., Legleiter, C. J., Overstreet, B. T., 2014. Early Results of Simultaneous Terrain and Shallow Water Bathymetry Mapping Using a Single-Wavelength Airborne LiDAR Sensor. *IEEE Journal of Selected Topics in Applied Earth Observations and Remote Sensing*, 7(2), 623-635.

Gangelhoff, J., Werner, C., Reiterer, A., 2023. Lightweight dual-wavelength bathymetric lidar for accurate seabed mapping. *Proc. SPIE 12621, Multimodal Sensing and Artificial Intelligence: Technologies and Applications III*, 126210I.

Kim, H., Jung, M., Lee, J., Wie, G., 2023. Progressive Gaussian Decomposition of Airborne Bathymetric LiDAR Waveform for Improving Seafloor Point Extraction. *Applied Sciences*, 13(19). https://www.mdpi.com/2076-3417/13/19/10939.

Kinzel, P., Legleiter, C., 2019. sUAS-Based Remote Sensing of River Discharge Using Thermal Particle Image Velocimetry and Bathymetric Lidar. *Remote Sensing*, 11, 2317.

Lague, D., Brodu, N., Leroux, J., 2013. Accurate 3d comparison of complex topography with terrestrial laser scanner: application to the rangitikei canyon (n-z).

Lague, D., Feldmann, B., 2020. Chapter 2 - topo-bathymetric airborne lidar for fluvial-geomorphology analysis. P. Tarolli, S. M. Mudd (eds), *Remote Sensing of Geomorphology*, Developments in Earth Surface Processes, 23, Elsevier, 25–54.

Mandlburger, G., Pfeifer, N., Wieser, M., Höfle, B., 2016a. Topo-bathymetric lidar for monitoring river morphodynamics: A case study at the pielach river. *ISPRS Archives*, XLI-B1, 933–940.

Mandlburger, G., Pfennigbauer, M., Schwarz, R., Flöry, S., Nussbaumer, L., 2020. Concept and Performance Evaluation of a Novel UAV-Borne Topo-Bathymetric LiDAR Sensor. *Remote Sensing*, 12(6), 986.

Mandlburger, G., Pfennigbauer, M., Wieser, M., Riegl, U., Pfeifer, N., 2016b. EVALUATION OF A NOVEL UAV-BORNE TOPO-BATHYMETRIC LASER PROFILER. *The International Archives of the Photogrammetry, Remote Sensing and Spatial Information Sciences*, XLI-B1, 933–939. https://isprs-archives.copernicus.org/articles/XLI-B1/933/2016/.

Mitchell, T., 2019. From pills to ramms. *Proceedings of the 20th Annual JALBTCX Airborne Coastal Mapping and Charting Technical Workshop*, South Bend, Indiana.

Quadros, N., Keysers, J., 2018. Emerging trends in bathymetric lidar technology. https://www.hydro-international.com/content/article/emerging-trends-in-bathymetric-lidar-technology.

SBG Systems, 2025. Uav-based lidar can measure shallow water depth. https://spectrum.ieee.org/uavbased-lidar-can-measure-shallow-water-depth.

Szafarczyk, A., Toś, C., 2023. The Use of Green Laser in LiDAR Bathymetry: State of the Art and Recent Advancements. *Sensors*, 23(1), 292. https://www.mdpi.com/1424-8220/23/1/292.

Wilder Young, J., 2017. Little topo-bathy lidar. https://lidarmag.com/2017/09/17/little-topo-bathy-lidar/.

Zuckerman, S., 2019. Pills 2.5: From design to operations. *Proceedings of the 20th Annual JALBTCX Airborne Coastal Mapping and Charting Technical Workshop*, South Bend, Indiana.